metals

MDPI

Article

Reduction Kinetics of Compact Hematite with Hydrogen from 600 to 1050 °C

Junguo He, Kejiang Li, Jianliang Zhang and Alberto N. Conejo *

School of Metallurgical and Ecological Engineering, University of Science and Technology Beijing, Beijing 100083, China
* Correspondence: aconejonava@hotmail.com

Abstract: Reduction of iron ores with hydrogen is a solution to replace fossil fuels. For this reason, it is important to discuss previous discrepancies. Some previous studies suggest a rate minimum with respect to temperature. Our research work indicates that a rate minimum can be avoided. Thermogravimetric isothermal reduction experiments were carried out from 600 to 1050 °C with pure reagent ferric oxide and hydrogen using a tubular furnace. The morphology and chemical composition of the initial sample, consisting of particulate hematite (Fe_2O_3), and the final product, consisting of metallic iron (Fe°), was defined using scanning electron microscopy (SEM) and X-ray diffraction (XRD). The reduction rate for the conversion from hematite to magnetite (Fe_2O_3 to Fe_3O_4) was the highest, around 5 %/min, decreasing to around 2–5%/min for the second stage of conversion from magnetite to wüstite (Fe_3O_4 to FeO). This reduction rate remains almost constant from about 20–80% reduction, decreasing to 0.3–1%/min for the completion of reduction from wüstite to metallic iron (FeO to Fe°). The reduction controlling mechanism was evaluated based on the calculated apparent activation energy and fitting the experimental data to one gas-solid reaction equation. Under the experimental conditions in this work, the reduction rate of pure hematite with hydrogen linearly increased with temperatures from 600 to 1000 °C, without a rate minimum in this temperature range. Above 1000 °C, the reduction rate decreased due to sintering phenomena. This result suggests a maximum reduction temperature of 1000 °C using pure hematite and hydrogen as the reducing gas. The reduction controlling mechanisms identified using hydrogen as a reducing gas were chemical reaction for the conversion from hematite to wüstite and diffusion control for the final reduction from wüstite to metallic iron. Since the reduction rate from wüstite to metallic iron is the one that affects the overall rate of reduction, overall changes in porosity were also evaluated. Finally, the reduction of wüstite is schematically described.

Keywords: hydrogen reduction; activation energy; rate of reduction; porosity; controlling mechanism

Citation: He, J.; Li, K.; Zhang, J.; Conejo, A.N. Reduction Kinetics of Compact Hematite with Hydrogen from 600 to 1050 °C. *Metals* **2023**, *13*, 464. https://doi.org/10.3390/met13030464

Academic Editor: Man Seung Lee

Received: 19 January 2023
Revised: 18 February 2023
Accepted: 20 February 2023
Published: 23 February 2023

1. Introduction

There is an urgent need to achieve carbon neutrality and replace fossil fuels with sustainably produced hydrogen as a reducing gas due to the significant amount of CO_2 emissions [1–3]. This is especially necessary in China where 90% of steel production is by the Blast Furnace/Basic Oxygen Furnace (BOF) route [4], that produces around 2 tons of CO_2 per each ton of liquid steel. Among the alternative methods to reduce CO_2 emissions is the increased production of Direct Reduced Iron (DRI) using green hydrogen [5]. There are many challenges involved in replacing fossil fuels with hydrogen. Besides its price, transportation and storage issues, the reduction of iron ores with hydrogen is endothermic and demands a higher consumption of energy. Tang et al. [6] reported that, in order to maintain the thermal load, the volume of hydrogen should be increased. Additionally, due to its lower density and higher diffusivity in comparison with CO, hydrogen's residence time in the high temperature zone of the reactor is much shorter, resulting in a lower utilization ratio. As a result of these limitations, it has been argued that hydrogen cannot fully replace fossil fuels.

The reduction of iron oxides is a topochemical process, from hematite (Fe_2O_3) to magnetite (Fe_3O_4) then wüstite (FeO) and finally metallic iron (Fe°). Wüstite is only stable above 570 °C. Reduction kinetics using hydrogen as the reducing gas has been reviewed recently by several authors, as will be discussed below [7–9].

Turkdogan and Vinters [10] reported three possible controlling mechanisms using hematite ore and found that the transition from one mechanism to another depended on the thickness of the product layer. Garg et al. [11] investigated the reduction rate of iron oxide particles using H_2-H_2O gas mixtures from 700 to 1100 °C, indicating that increasing water vapor shifted the controlling mechanism from chemical reaction to diffusion control. Moon et al. [12] measured the reduction rate of hematite compact in the temperature range from 800 to 950 °C using H_2-CO gas mixtures, indicating higher rates of reduction with hydrogen. Lin et al. [13] were able to reproduce their experimental data using a two-dimensional nucleation model. Bahgat and Khedr [14] reported an increment in the reduction rate from 900 to 1100 °C and solid state diffusion as the controlling mechanism.

Several investigations have reported a minimum value on the rate of reduction as a function of temperature. El-Geassy and Nasr [15] studied the rate of reduction in the temperature range from 500 to 1100 °C, observing a minimum reduction rate at 650 °C. Moukassi et al. [16] reported a decrease in the reduction rate at 700 °C and a minimum reduction rate at 890 °C. Yi et al. [17] reported a minimum reduction rate at 950 °C but continued to increase above this temperature. The phenomena responsible for the rate minimum has been attributed to sintering. Turkdogan et al. [18] studied the pore structure of iron in hydrogen-reduced hematite, indicating that most of the pores in the reduced iron are connected to each other. At high temperature, the pores are large and few in number. Pineau et al. [19] reported sintering when the reduction temperature was higher than 750 °C. Yang et al. [20,21] reported that sintering started at 700 °C. As sintering occurs, diffusion becomes a rate limiting step. St. John and Hayes [22] found that the presence of a small amount of water vapor densified the structure of the product iron and slowed down the reaction rate. Similar results were reported by Moukassi [23], who found that the presence of a small amount of water vapor (2.5%) significantly slowed down the reduction rate. This was attributed to the adsorption of water. Jung and Jai Lee [24] also reported similar results.

The reduction rate of hydrogen is higher in comparison to CO. Rodriguez et al. [25] compared the reduction rate of pure hematite with H_2-CO at low temperatures (550 to 650 °C) and found that only pure hydrogen could achieve 100% reduction and higher rates increasing H_2 in the gas mixture. Fruehan et al. [26] reported a maximum conversion from 81% to 93% at 600 °C with pure hydrogen, using commercial iron ores. A higher conversion corresponded to iron ore with a smaller particle size. The decrease in the reduction rate was attributed to the formation of a dense iron layer around wüstite.

Spreitzer and Schenk [7] summarized activation energies for the reduction of iron oxides with hydrogen, reporting a range from 11 to 246 kJ/mol. Such a large range is due to different experimental conditions involving different temperatures, gas flow rate, particle size, iron ore composition, etc. The summary of activation energies reported by Heidari et al. [8] also indicate that, in general, increasing hydrogen in the gas mixture decreases the activation energy.

Ma et al. [27] have discussed the challenges, at the microscopic scale, to better understand the reduction mechanisms with hydrogen, in particular the role of defects (cracks, pores, vacancies, dislocations, etc.) and reaction kinetics. The tools available are still insufficient: for example, Ab initio molecular dynamics (AIMD) is limited to a few hundred atoms and Reactive force field molecular dynamics (ReaxFF-MD) can be used to study chemical reactions with a few million atoms.

In spite of the significant amount of previous research on the reduction rate of iron oxides with hydrogen, there is still a need for better understanding of the reaction mechanisms due to the large number of variables involved, such as reduction temperature, chemical composition of reducing gas, chemical composition of iron oxide/iron ore, including its gangue content, porosity, particle size, pressure, etc. This work focuses on the measurement of reduction rates, the definition of the reaction mechanism for the reduction of pure hematite with hydrogen in the temperature range from 600 to 1050 °C, and the identification of the conditions that lead to a lower reduction rate in the temperature range investigated.

2. Materials and Methods

The hematite powder used in the experimental work is an analytically pure reagent with an average particle size of 74 µm, produced by Sinopharm Chemical Reagent Co., Ltd. (Purity $\geq$ 99%, Shanghai, China). The particle size has a significant influence on the rate of reduction. Industrial iron ore concentrate should have a maximum particle size of 106 microns [28], providing a minimum surface area of 1800 cm^2/g. The particle size of the hematite used in this study is close in size and surface area to an industrial iron ore concentrate.

The powder was mixed with 7% distilled water and compacted with a pressure of 10 MPa to form cylinders with a diameter of 10 mm, a height of 14 mm and weight of 3 g. The cylinders were then dried at 105 $\pm$ 5 °C for 4 h. The phase analysis of the initial sample was obtained using X-ray diffraction (XRD) with an Ultima-IV apparatus (3 KW, 40 kV/40 mA, Cu, λ = 1.5406 Å) manufactured by Japanese Neo-Confucianism, and the morphology was examined at 1000$\times$ using a scanning electron microscope (SEM; Carl ZEISS NTS, JSM-6510, 20Kv, WD = 10.0 mm), as shown in Figure 1. Upon comparison of the X-ray diffraction pattern of the sample with the standard defined by the National Bureau of Standards [29], it was confirmed that the sample was high purity hematite. Sample preparation for SEM was carried out by mounting the sample in epoxy resin, using a 2:1 ratio of resin to coagulant, and then polished with sand paper and diamond polishing paste, avoiding any overheating which could modify the original texture.

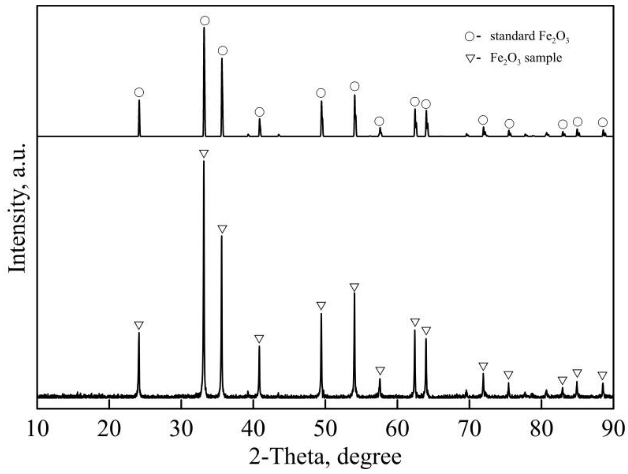

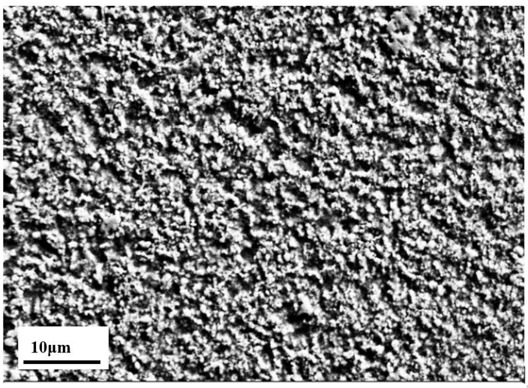

Figure 1. (**Upper**) XRD pattern of initial sample, (**Bottom**) Morphology of initial sample.

The tubular reduction furnace is shown in Figure 2. The furnace consists of three parts: tube resistance main furnace, gas flow control instrument and data collector. The mass of the sample is recorded by an electronic balance with an accuracy of 1µg, placed on a platform on top of the furnace. The data are recorded automatically by the computer. The basket attached to the lower end of the electronic balance is made of molybdenum wire.

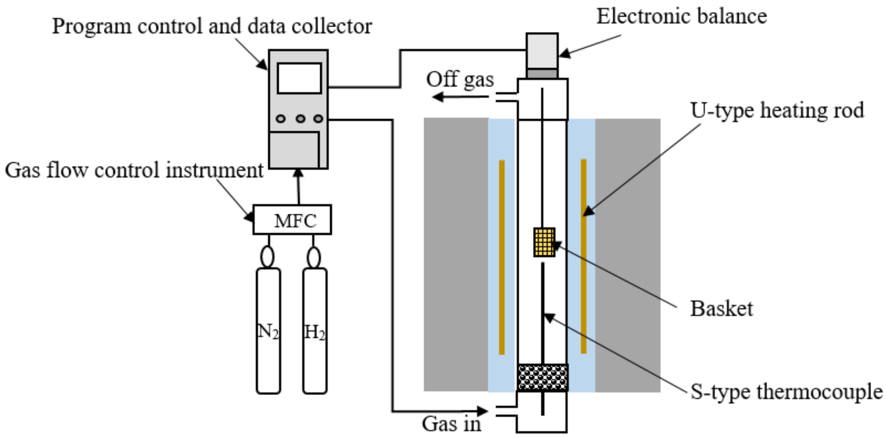

Figure 2. Experimental equipment for hydrogen reduction.

All experiments were carried out under isothermal conditions. Initially, the furnace was heated using 3Nl/min of high-purity nitrogen. After reaching the specified reduction temperature, the samples were kept at this temperature for 5 min before H_2 was introduced at a flow rate of 3.0 Nl/min. After the weight of the sample remained constant, it was cooled to room temperature under the protection of nitrogen. The temperature range of the experimental work was from 600 to 1050 °C at temperature intervals of 50 °C.

3. Results and Discussion

3.1. Reduction Kinetics

The results from this work consist of the reduction degree as a function of time for different temperatures under isothermal conditions using pure hematite and pure hydrogen. To evaluate the reduction kinetics, the reduction degree is plotted as a function of time. The rates of conversion are obtained from the slopes in those plots. The activation energies are subsequently calculated using an Arrhenius analysis that can allow the estimation of possible reaction mechanisms.

The reduction degree (α) is defined as a ratio between the changes of mass due to removal of oxygen (initial mass minus mass as a function of time) with respect to the total change of mass after the reduction process is completed, as follows:

$$\alpha\ (\%) = \frac{M_o - M_t}{M_o - M_\infty} \times 100, \tag{1}$$

where M_0 is the initial sample mass, M_t is the sample mass as a function of time and M_∞ is the mass once the sample is reduced completely.

Figure 3 shows the reduction degree as a function of temperature. It has been divided into two parts to better illustrate the reduction behavior at low and high temperatures. The first stage of reduction, corresponding to a reduction degree from 0 to 11.1%, hematite is converted to magnetite (Fe_2O_3 to Fe_3O_4), the reduction rate is around 5 %/min between 600 and 800 °C. In this temperature range and for a reduction degree from about 20 to 80%, the reduction rate is approximately linear with time, about 2 to 5 %/min. This range in the reduction degree covers the conversion from magnetite to wüstite ($Fe_3O_4 \rightarrow FeO$) and part of the conversion from wüstite to metallic iron ($FeO \rightarrow Fe$). The final conversion from wüstite to metallic iron, above 90% reduction, shows a lower reduction rate (0.3–1%/min) at all temperatures.

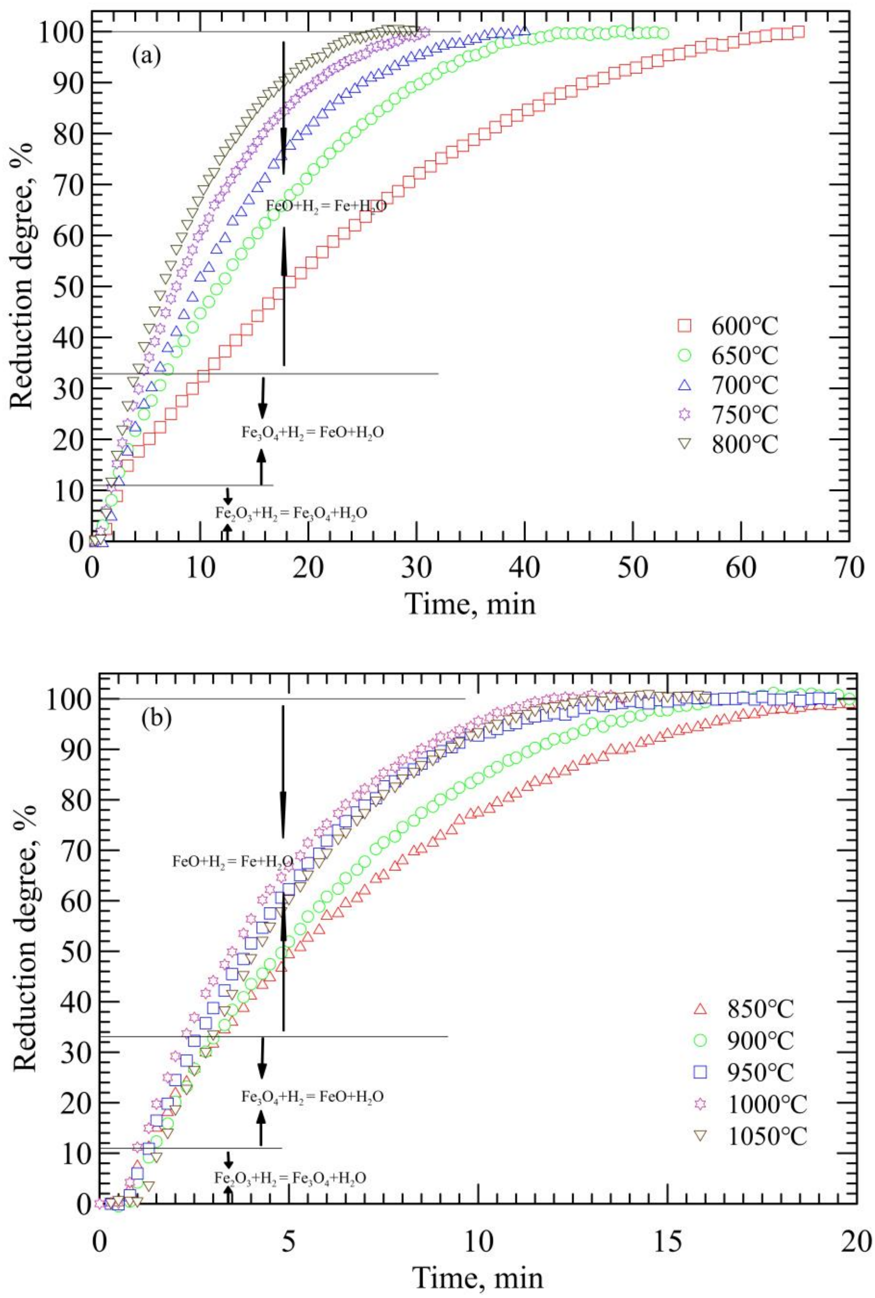

Figure 3. Reduction degree of pure hematite with hydrogen. (**a**) 600–800 °C; (**b**) 850–1050 °C.

The reduction rate Increases from around 0.3%/min at 600 °C to 1%/min at 800 °C. As can be seen from the figure, the rate ranges from 2% to 5%/min up to about 80% conversion. The change in slope is an indication of a change in the reaction controlling mechanisms.

The activation energy is computed using the Arrhenius expression:

$$k(T) = A\ \exp\left(-\frac{E_a}{RT}\right) \tag{2}$$

where k is a rate constant that only depends on temperature and whose units depend on the order of reaction (s^{-1} for first order reactions), A is a pre-exponential term with similar units to k, E_a is the activation energy in kJ/mol and R is the gas constant in kJ/mol·K. In the Arrhenius method used to compute the activation energy, Equation (2) is linearized. A plot 1/T versus k(T) in log scales yields a slope equal to E_a.

The rate of reduction in a gas-solid reaction ($A_{(g)}$ + $bB_{(s)}$ $\rightarrow$ products) and the rate constant are related by the following expression [30]:

$$\frac{d\alpha}{dt} = bkC_A(1-\alpha) \tag{3}$$

where α is the fractional conversion of the solid B, b is a stoichiometric coefficient, k is the rate constant and C_A is the concentration of the reducing gas in mol/m^3. If the Arrhenius analysis is based on the rate of conversion ($d\alpha/dt$) instead of the rate constant (k), the activation energy is called apparent activation energy. As can be seen in Figures 3 and 4, there are three different regions: the first one corresponds to the conversion from hematite to magnetite; the second slope includes the conversion of magnetite to wüstite and also part of the conversion from wüstite into metallic iron; and the final stage shows a progressive decrease in the rate of reduction that corresponds to the final conversion from wüstite to metallic iron. It can also be observed that, for each reduction temperature, it is possible to identify one single slope for a range in the conversion degree from 20–80%. Therefore, these slopes are employed to characterize the whole conversion process from hematite to metallic iron in the present investigation. The slopes are taken from Figure 4 and Table 1 summarizes the average reduction rate at different temperatures. With this information it is possible to obtain the activation energies using the Arrhenius analysis.

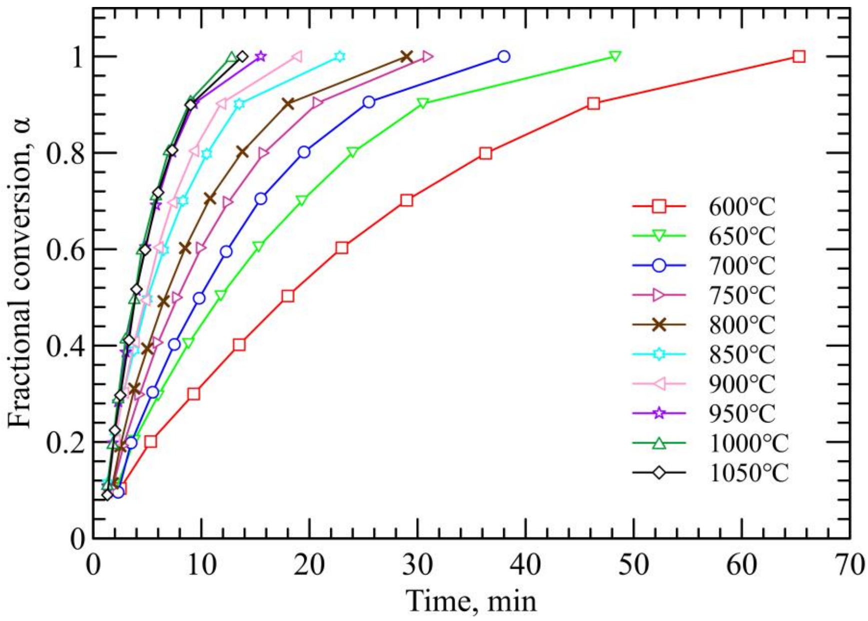

Figure 4. Fractional conversion as a function of time and temperature.

Table 1. Data for the Arrhenius analysis.

T, °C	Rate, (%/min)	ln Rate, (min^{-1})	1/T, (K^{-1})
600	1.93	0.66	1.15×10^{-3}
650	2.96	1.08	1.08×10^{-3}
700	3.77	1.33	1.03×10^{-3}
750	4.67	1.54	9.79×10^{-4}
800	5.41	1.69	9.33×10^{-4}
850	6.78	1.91	8.98×10^{-4}
900	8.22	2.11	8.54×10^{-4}
950	10.97	2.40	8.19×10^{-4}
1000	11.72	2.46	7.87×10^{-4}
1050	10.97	2.40	7.57×10^{-4}

From Figure 5, the apparent activation energy is 36.69 kJ·mol^{-1}. The value of activation energy is commonly employed to suggest the controlling reaction mechanisms. Previous reports [31,32] suggest that an effective activation energy in the range from 8 to 28 kJ /mol define a gas diffusion controlling mechanism; in the range from 28 to 40 kJ/mol, this can be a mixed controlling mechanism (both chemical reaction and gas diffusion) and from 40 to 300 kJ/mol, this can be a solid state controlling mechanism. In accordance with those guidelines, for the current experimental conditions, the reduction of the pure hematite block can be controlled by both chemical reaction and gas internal diffusion.

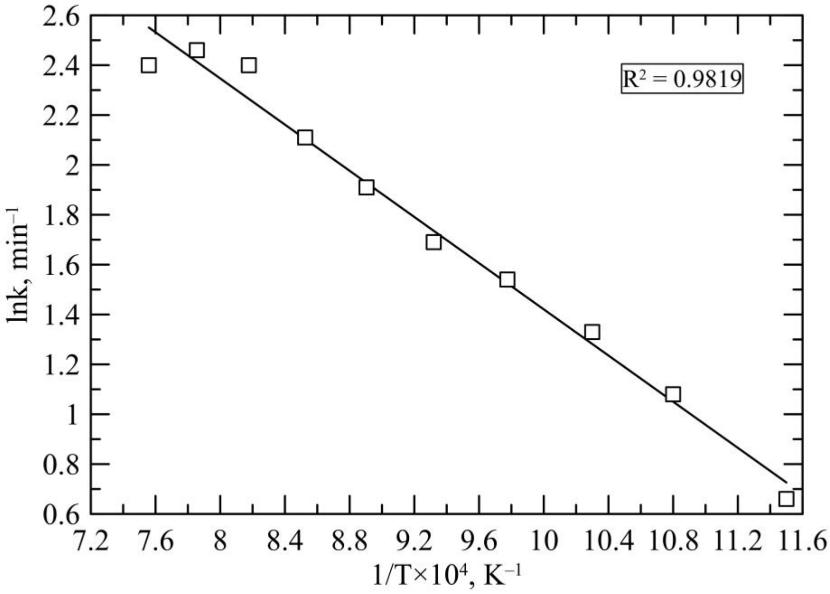

Figure 5. Calculation of activation energy using Arrhenius equation.

Rates of diffusion and chemical reactions both increase with temperature and, therefore, a positive effect of temperature would be expected. Figure 6 clearly illustrates that the reduction rate increases with temperature, almost linearly from 600 to 950 °C, decreasing after 950 °C. In other words, the maximum reduction temperature of pure hematite using pure hydrogen should be 950 °C.

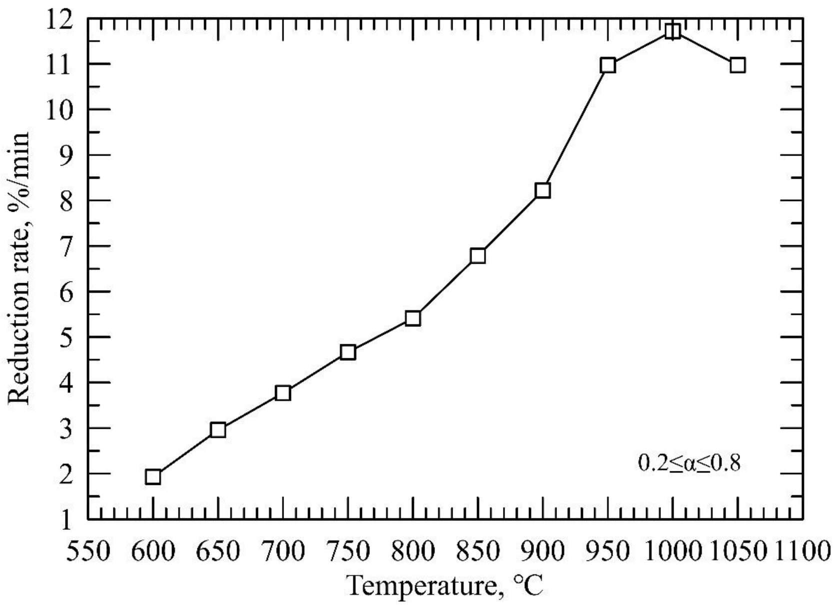

Figure 6. Reduction rate of pure hematite as a function of temperature.

It is clear from the changes in the slope in Figure 3 that there are three reaction mechanisms during the conversion of hematite into metallic iron. The activation energy increases, with the highest value for the last stage of conversion. Under similar conditions, and for the reduction of pure hematite with hydrogen, El-Geassy et al. [33] reported an activation energy of 28.7 kJ/mol for the first stage of reduction in the temperature range from 700 to 1050 °C, increasing when the reduction degree was higher than 70% to 59.6 kJ/mol in the temperature range from 700 to 900, and 168.4 kJ/mol when the temperature was further increased from 950 to 1050 °C. The values on activation energy are highly variable because they depend on the specific experimental conditions. For example, for the conversion of hematite to magnetite a range from 33.28 kJ/mol to 139.2 kJ/mol has been reported [34], indicating different reaction mechanisms. Table 2 provides a short summary of activation energies for the reduction of iron oxides. It can be observed that, for the same reducing gas and temperature range, the activation energy can be significantly different due to changes in porosity [35].

Table 2. Activation energies for the reduction of iron oxides.

Iron Oxides	Reducing Gas	Temperature	E_a [kJ/mol]	Ref.
$Fe_2O_3 \rightarrow Fe_3O_4$	5%H_2 + 95%N_2	Non-isothermal, <325 °C	89.1	[13]
	67%H_2 + Ar	Non-isothermal, 290–480 °C	124	[36]
	5%CO + Ar	Isothermal, 25–700 °C	33–74	[37]
$Fe_3O_4 \rightarrow Fe$	5%H_2 + 95%N_2	Non-isothermal, <325 °C	70	[13]
	(25–100%H_2) + He	Isothermal, 310 and 377 °C	60.7	[38]
$Fe_2O_3 \rightarrow Fe$	100% H_2	Isothermal, 700–1100 °C Porosity 7%	53.5	[35]
	100% H_2	Isothermal, 700–1100 °C Porosity 35%	21.5	[35]

In order to define a kinetic model through model fitting, Vyazovkin et al. [39] provided useful recommendations to process the experimental data. Model fitting is based on the general function for the rate of conversion, that indicates that it depends on the temperature and the degree of conversion (at constant pressure):

$$\frac{d\alpha}{dt} = k(T)\, f(\alpha) \tag{4}$$

where $f(\alpha)$ is function that depends on the degree of conversion. The previous equation can also be expressed as follows, by replacing the value of k(T):

$$\frac{d\alpha}{dt} = A\ \exp\left(-\frac{E_a}{RT}\right)\, f(\alpha) \tag{5}$$

The integrated expression defines a new function called $g(\alpha)$, or integral form of a reaction model:

$$g(\alpha) = \int_0^{\alpha} \frac{d\alpha}{f(\alpha)} = \int_0^{t} k dt = A \int_0^{t} \exp\left(-\frac{E_a}{RT}\right) dt = kt \tag{6}$$

There are a significant number of kinetic models. The values of kt are fitted with a model, considering in principle that all models can fall into three different groups [39]: accelerating, decelerating and sigmoidal. Reduction falls in the group of decelerating models. Figure 7 shows that the current experimental data can be described by the contracting cylinder model:

$$g(\alpha) = 1 - (1-\alpha)^{\frac{1}{2}} \tag{7}$$

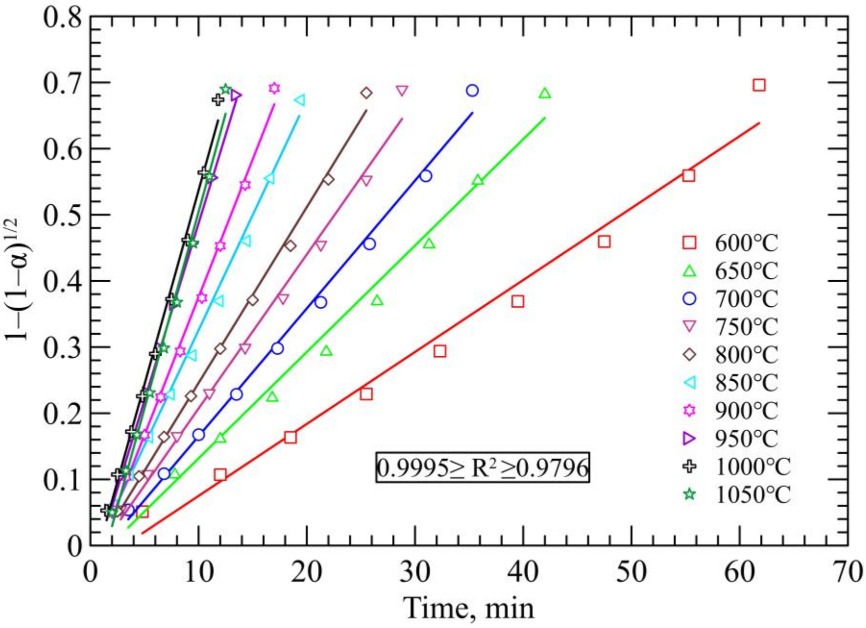

Figure 7. Model fitting of experimental data to a reaction mechanism.

3.2. Morphology Analysis

The morphological changes due to the reduction of hematite particles with hydrogen at different temperatures were observed using SEM at a magnification of 1000×, as shown in Figure 8. The samples reduced from 600 to 750 °C show different degrees of porosity, that start decreasing above 750 °C due to sintering. Sintering keeps increasing until 950 °C. However, due the rise in temperature, the rate of reduction also keeps increasing. The rate minimum reported in previous investigations [15,21,33,35,40] below 950 °C was not observed under the current experimental conditions. The reduction rate decelerates above 950 °C due to sintering and the transformation from α-Fe $\rightarrow$ γ-Fe, that involves the formation of a denser structure, shifting the reaction controlling mechanism from chemical reaction control to diffusion control [41]. The phase transformation for pure iron occurs at 910 °C, with an increment in density from 7875 to 8099 kg/m^3 [42]. At temperatures above 1000 °C, diffusion of hydrogen through the sintered and denser iron layer, as well as diffusion of water vapor out from the wüstite/iron interface, contributes to decreasing the overall rate of reduction. Image-J software was used to calculate the average porosity from 2D SEM images. This method provided similar results in comparisons with helium pycnometry and mercury porosimetry [43]. Figure 9 shows the changes in porosity as temperature increases schematically.

The porosity in the samples was measured using image analysis, obtaining a continuous decrease in porosity as temperature increased from around 61% at 600 °C to 55%, 53% and 49% at 950 °C, 1000 °C and 1050 °C, respectively. El-Geassy and Nasr [15] reported a decrease in porosity in 90% reduced hematite compacts with hydrogen from around 70% at 500 °C to 50% at around 1100 °C. Turkdogan et al. [18] reported a decrease in the pore surface area of high-grade hematite ore with hydrogen from 39 m^2/g at 200 °C to 0.1 m^2/g at 1200 °C.

Results indicate that reducing pure hematite with hydrogen gives a linear increment in the rate of reduction from 600 to 1000 °C, without any rate minimum in that temperature range, despite sintering also continuously increasing, indicating a dominant role of temperature on the kinetics of reduction. This result would suggest that a rate minimum could be obtained using iron ores with additives that promote a different sintering behavior.

Figure 10 shows the progress at the reaction interface for different degrees of reduction (30% to 80%) at 950 °C. It can be observed that the sample is progressively reduced with the reducing gas penetrating inside the inner regions of the sample due to a high rate of diffusion of the reducing gas. However, due to sintering, the center is topo-chemically reduced, switching to a diffusion-controlled process. The diffusion of both hydrogen and water vapor decreases at the latter stages of reduction; water vapor also might contribute to sintering due to increases in the plasticity of wüstite [15,16]. Using EDS, the bright color was identified as metallic iron and the dark color as wüstite.

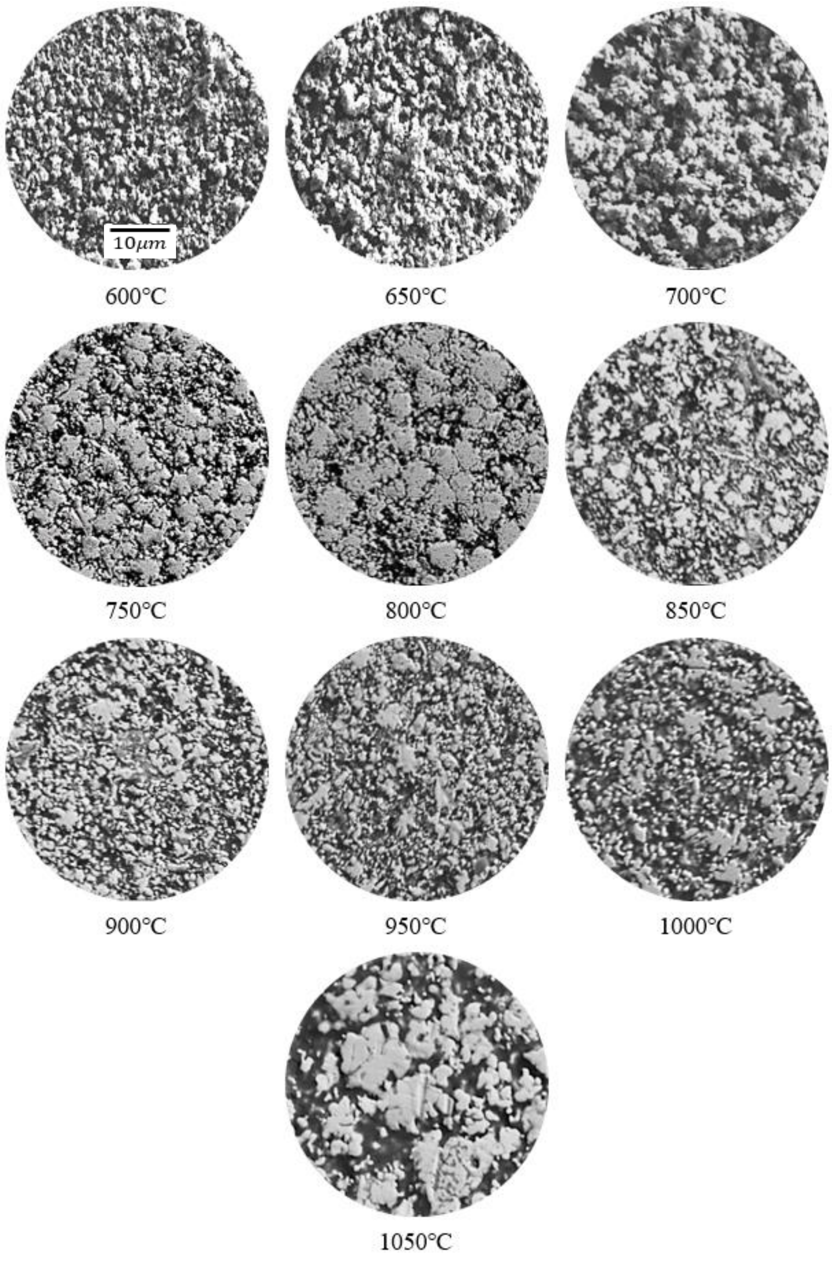

Figure 8. Morphology of the product after complete reduction at different temperatures at 1000×. White area is reduced metallic iron.

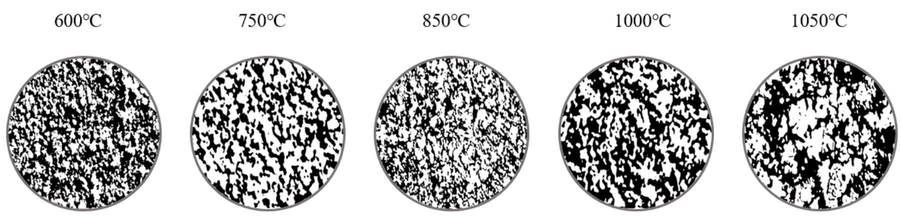

Figure 9. Changes in porosity of reduced samples as a function of temperature. Black areas indicate pores.

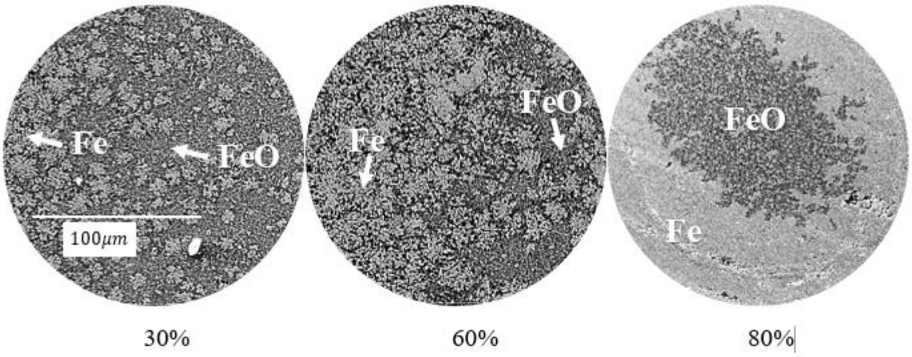

Figure 10. Morphology at a constant reduction temperature of 950 °C and three stages of reduction (30%, 60% and 80%). Note: The bright color is Fe and the gray color is FeO.

Figure 11 is a schematic representation of the final stage of reduction. This stage is the most critical because it is the slowest stage. Edstrom [44] suggested solid state diffusion of iron and oxygen ions. The mechanism proposed in this figure includes the diffusion of hydrogen and water vapor through the iron layer and three reactions at the wüstite/iron interface: hydrogen dissociates into hydrogen ions and releases electrons, the electrons combine with iron ions to form metallic iron and the hydrogen ions with oxygen ions to form water vapor. The iron phase represented is austenite with a face centered cubic structure that has an interatomic distance of 3.64 Å. This distance allows the diffusion of water molecules that have a diameter of 2.84 Å. [45] The whole process involves diffusion of reactant gas to the reaction interface, dissociation into ions of reactants (solid and gas), chemical reactions at the interface and diffusion of the reaction products.

$$FeO_{(s)} = Fe^{2+} + O^{2-}$$

$$H_{2(g)} = 2H^{+} + 2e^{-}$$

$$Fe2^{+} + 2e^{-} = Fe^{o}_{(s)}$$

$$O^{2-} + 2H^{+} = H_2O_{(g)}$$

Overall reaction: $FeO_{(s)} + H_{2(g)} = Fe^{o}_{(s)} + H_2O_{(g)}$.

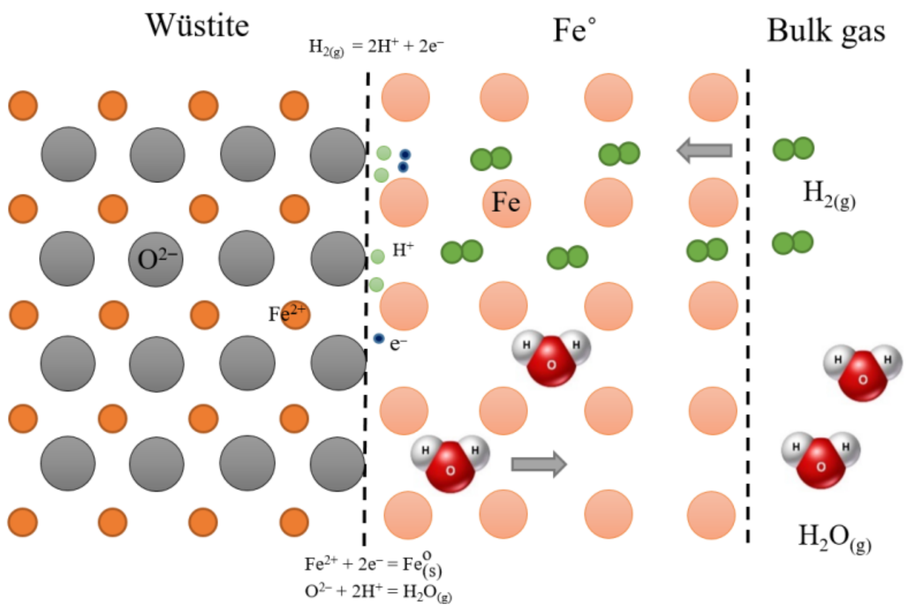

Figure 11. Schematic representation of the reduction of wüstite with hydrogen.

4. Conclusions

Challenges remain with hydrogen reduction of iron ores. This is not only on the part related to the production of cheaper green hydrogen but also due to the complexity of the reduction process affected by so many variables.

In this work, the isothermal reduction of pure hematite compacts with pure hydrogen was carried out in the temperature range from 600 to 1050 °C. The experimentally measured activation energy was 36.6 kJ/mol indicating a mixed control mechanism, chemical control at the reaction interface during the initial and middle part of the reduction process shifting to diffusion control at the end due to sintering. The reduction rate linearly increased from 600 °C to 1000 °C without a rate minimum, as has been suggested in previous investigations. The reduction rate decreased above 1000 °C due to sintering and the resultant decrease in porosity and the formation of a denser structure. This result indicates that a rate minimum can be avoided in the temperature range from 600 °C to 1000 °C, reducing high purity hematite with hydrogen. It also suggests that the mineralogical species in iron ores could be responsible for the rate minimum reported in previous investigations.

The final stage of reduction, from wüstite to metallic iron, is the slowest step and the one that constrains the whole process. The evidence for the lower reduction rates indicates sintering phenomena that open the way for further research to inhibit such phenomena.

Author Contributions: Conceptualization, methodology, investigation, writing—original draft preparation, writing—review and editing, supervision, formal analysis, A.N.C.; experimental work, data processing, investigation, preliminary analysis, review and editing, J.H.; review and editing, K.L.; funding acquisition, J.Z. All authors have read and agreed to the published version of the manuscript.

Funding: AC acknowledges the financial support from the Fundamental Research Funds (Grant No. 06500108) from the University of Science and Technology Beijing, China.

Data Availability Statement: Not applicable.

Conflicts of Interest: The authors declare no conflict of interest.

References

1. Holappa, L. A general vision for reduction of energy consumption and CO_2 emissions from the steel industry. *Metals* **2020**, *10*, 1117. [CrossRef]
2. Fan, Z.; Friedmann, S.J. Low-carbon production of iron and steel: Technology options, economic assessment, and policy. *Joule* **2021**, *5*, 829–862. [CrossRef]
3. Kim, J.; Sovacool, B.K.; Bazilian, M.; Griffiths, S.; Lee, J.; Yang, M.; Lee, J. Decarbonizing the iron and steel industry: A systematic review of sociotechnical systems, technological innovations, and policy options. *Energy Res. Soc. Sci.* **2022**, *89*, 102565. [CrossRef]
4. Pan, C.; Pang, J.M. Development trace and application prospect of hydrogen metallurgy technology. *China Metall.* **2021**, *31*, 73–77.
5. Zhang, B.; Zhao, Z.; Guo, H.; Quan, Q.; Xue, Q. Development of direct- reduction ironmaking technology in gas-based shaft furnace. *Res. Iron Steel* **2016**, *44*, 59–62.
6. Tang, J.; Chu, M.S.; Li, F.; Feng, C.; Liu, Z.G.; Zhou, Y.S. Development and progress on hydrogen metallurgy. *Int. J. Miner. Metall. Mater.* **2020**, *27*, 713–723. [CrossRef]
7. Spreitzer, D.; Schenk, J. Reduction of Iron Oxides with Hydrogen—A Review. *Steel Res. Int.* **2019**, *90*, 1900108. [CrossRef]
8. Heidari, A.; Niknahad, N.; Iljana, M.; Fabritius, T. A review on the kinetics of iron ore reduction by hydrogen. *Materials* **2021**, *14*, 7540. [CrossRef]
9. Ma, Y.; Souza Filho, I.R.; Bai, Y.; Schenk, J.; Patisson, F.; Beck, A.; van Bokhoven, J.A.; Willinger, M.G.; Li, K.; Xie, D.; et al. Hierarchical nature of hydrogen-based direct reduction of iron oxides. *Scr. Mater.* **2022**, *213*, 114571. [CrossRef]
10. Turkdogan, E.T.; Vinters, J.V. Gaseous reduction of iron oxides Part I. Reduction of hematite in hydrogen. *Metall. Trans.* **1971**, *2*, 3175–3188. [CrossRef]
11. Garg, P.; Hu, X.; Li, Y.; Li, K.; Nag, S.; Zhang, J. Kinetics of Iron Oxide Reduction in H_2/ H_2O Gas Mixture: Global and Stepwise Reduction. *Metall. Mater. Trans. B Process. Metall. Mater. Process. Sci.* **2022**, *53*, 1759–1774. [CrossRef]
12. II-Joon, M.; Chang-Hee, R.; Dong-Joon, M. Reduction of hematite compact by H_2-CO gas mixtures. *Steel Res.* **1998**, *69*, 302–306.
13. Lin, H.-Y.; Chen, Y.-W.; Li, C. The mechanism of reduction of iron oxide by hydrogen. *Thermochim. Acta* **2003**, *400*, 61–67. [CrossRef]
14. Bahgat, M.; Khedr, M.H. Reduction kinetics, magnetic behavior and morphological changes during reduction of magnetite single crystal. *Mater. Sci. Eng. B* **2007**, *138*, 251–258. [CrossRef]
15. El-Geassy, A.A.; Nasr, M.I. Influence of the original structure on the kinetics of hydrogen reduction of hematite compacts. *Trans. Iron Steel Inst. Jpn.* **1988**, *28*, 650–658. [CrossRef]

16. Rao, Y.K.; Moinpour, M. Kinetics of reduction of hematite with hydrogen gas at modest temperatures. *Metall. Trans. B* **1983**, *14*, 711–723. [CrossRef]
17. Yi, L. Fundamental Research on Gas-based DirectReduction of Iron Ore Pellets with Carbon Monoxide and Hydrogen Mixtures. Doctoral Dissertation, Central South University, Changsha, China, 2013.
18. Turkdogan, E.T.; Olsson, R.G.; Vinters, J.V. Gaseous reduction of iron oxides: Part II. Pore characteristics of iron reduced from hematite in hydrogen. *Metall. Mater. Trans. B* **1971**, *2*, 3189–3196. [CrossRef]
19. Pineau, A.; Kanari, N.; Gaballah, I. Kinetics of reduction of iron oxides by H_2. Part II. Low temperature reduction of magnetite. *Thermochim. Acta* **2007**, *456*, 75–88. [CrossRef]
20. Yang, X. A Study of The Reduction Kinetics of Iron Oxide with H_2-rich Gas. Ph.D. Thesis, University of Science and Technology Beijing, Beijing, China, 2016.
21. Yang, X.B.; Hu, X.J.; Chen, Z.Y.; Dang, J.; Fang, F.; Chou, K.C. Structure evolution in the reduction process of FeO powder by hydrogen. *Gongcheng Kexue Xuebao/Chin. J. Eng.* **2015**, *37*, 163–167.
22. John, D.H.S.; Hayes, P.C. Microstructural features produced by the reduction of wustite in H_2/H_2O gas mixtures. *Metall. Trans. B* **1982**, *13*, 117–124. [CrossRef]
23. Moukassi, M.; Gougeon, M.; Steinmetz, P.; Dupre, B.; Gleitzer, C. Hydrogen reduction of wustite single crystals doped with Mg, Mn, Ca, Al, and Si. *Metall. Trans. B* **1984**, *15*, 383–391. [CrossRef]
24. Jung, S.S.; Lee, J.S. In-situ kinetic study of hydrogen reduction of Fe_2O_3 for the production of Fe nanopowder. *Mater. Trans.* **2009**, *50*, 2270–2276. [CrossRef]
25. Rodriguez, R.; Bedolla, E.; Conejo, A. Kinetics of Reduction of Fe_2O_3 Particles with H_2-CO Mixtures at Low Temperalures. *Iron Steelmak.* **2003**, *1*, 25–33.
26. Fruehan, R.J.; Li, Y.; Brabie, L.; Kim, E.J. Final stage of reduction of iron ores by hydrogen. *Scand. J. Metall.* **2005**, *34*, 205–212. [CrossRef]
27. Kim, S.H.; Zhang, X.; Ma, Y.; Souza Filho, I.R.; Schweinar, K.; Angenendt, K.; Vogel, D.; Stephenson, L.T.; El-Zoka, A.A.; Mianroodi, J.R.; et al. Influence of microstructure and atomic-scale chemistry on the direct reduction of iron ore with hydrogen at 700 °C. *Acta Mater.* **2021**, *212*, 116933. [CrossRef]
28. Abazarpoor, A.; Halali, M.; Hejazi, R.; Saghaeian, M. HPGR effect on the particle size and shape of iron ore pellet feed using response surface methodology. *Miner. Process. Extr. Metall. Trans. Inst. Min. Metall.* **2018**, *127*, 40–48. [CrossRef]
29. Morris, M.; McMurdie, H.; Evans, E.; Peretzkin, B.; Parker, H.; Panagiotopoulos, N. Standard X-ray diffractin powder patterns. Section 18. *Natl. Bur. Stand.* **1981**, *18*, 37.
30. Kimura, S.; Takagi, Y.; Tone, S.; Otake, T. A rate equation for gas-solid reactions accounting for the effect of solid structure and its application. *J. Chem. Eng. Jpn.* **1981**, *14*, 456–461. [CrossRef]
31. Li, L.; Niu, L.; Guo, H.J.; Duan, S.-C.; Li, Y.-Q.; Meng, X.-L. Experimental research and kinetics analysis on hydrogen reduction of limonite. *Gongcheng Kexue Xuebao/Chin. J. Eng.* **2015**, *37*, 13–19.
32. Liu, J.; Zhang, J.; Zhou, T. Assessment of Apparent Activation Energies for Reduction Reactions of Iron Oxides by Hydrogen. *J. Iron Steel Res. Int.* **1999**, *11*, 9–13.
33. El-Geassy, A.A. Gaseous reduction of Fe_2O_3 compacts at 600 to 1050 °C. *J. Mater. Sci.* **1986**, *21*, 3889–3900. [CrossRef]
34. Yu, J.; Han, Y.; Li, Y.; Gao, P.; Li, W. Mechanism and kinetics of the reduction of hematite to magnetite with CO–CO_2 in a micro-fluidized bed. *Minerals* **2017**, *7*, 209. [CrossRef]
35. El-Geassy, A.A.; Shehata, K.A.; Ezz, S.Y. Mechanism of Iron Oxide Reduction with Hydrogen/Carbon Monoxide Mixtures. *Trans. ISIJ* **1977**, *17*, 629–635. [CrossRef]
36. Wimmers, O.J.; Arnoldy, P.; Moulijn, J.A. Determination of the reduction mechanism by temperature-programmed reduction: Application to small iron oxide (Fe_2O_3) particles. *J. Phys. Chem.* **1986**, *90*, 1331–1337. [CrossRef]
37. Shimokawabe, M.; Furuichi, R.; Ishii, T. Influence of the preparation history of α-Fe_2O_3 on its reactivity for hydrogen reduction. *Thermochim. Acta* **1979**, *28*, 287–305. [CrossRef]
38. Moinpour, M.; Rao, Y.K. Kinetics of reduction of hematite with He-H_2 gas mixtures at moderate temperatures. *Trans. ISIJ* **1988**, *28*, 714–720. [CrossRef]
39. Vyazovkin, S.; Burnham, A.K.; Criado, J.M.; Pérez-Maqueda, L.A.; Popescu, C.; Sbirrazzuoli, N. ICTAC Kinetics Committee recommendations for performing kinetic computations on thermal analysis data. *Thermochim. Acta* **2011**, *520*, 1–19. [CrossRef]
40. Moukassi, M.; Steinmetz, P.; Dupre, B.; Gleitzer, C. A study of the mechanism of reduction with hydrogen of pure wustite single crystals. *Metall. Trans. B* **1983**, *14*, 125–132. [CrossRef]
41. Nicolle, R.; Rist, A. The mechanism of whisker growth in the reduction of wüstite. *Metall. Trans. B* **1979**, *10*, 429–438. [CrossRef]
42. Cho, Y.G.; Kim, J.Y.; Cho, H.H.; Cha, P.R.; Suh, D.W.; Lee, J.K.; Han, H.N. Analysis of transformation plasticity in steel using a finite element method coupled with a phase field model. *PLoS ONE* **2012**, *7*, e35987. [CrossRef]
43. Andreola, F.; Leonelli, C.; Romagnoli, M. Techniques Used to Determine Porosity. *Am. Ceram. Soc. Bull.* **2000**, *79*, 49–52.
44. Edstrom, J.O. The mechanism of reduction of iron oxides. *J. Iron Steel Inst.* **1953**, *175*, 289–304.
45. Pashley, R.; Israelachvili, J. Molecular layering of water at surfaces and origin of repulsive hydration forces. *Nature* **1983**, *306*, 2.